Observation of room-temperature magnetic skyrmions in Pt/Co/W structures with a large spin-orbit coupling

T. Lin,[1] H. Liu,[2] S. Poellath,[3] Y. Zhang,[4] B. Ji,[1] N. Lei,[1,*] J. J. Yun,[5] L. Xi,[5] D. Z. Yang,[5] T. Xing,[1] Z. L. Wang,[1] L. Sun,[2,6] Y. Z. Wu,[2] L. F. Yin,[2] W. B. Wang,[2] J. Shen,[2] J. Zweck,[3] C. H. Back,[3,7,†] Y. G. Zhang,[1] and W. S. Zhao[1,‡]

[1]*Fert Beijing Institute, BDBC, School of Electronic and Information Engineering, Beihang University, Beijing 100191, China*
[2]*Department of Physics and State Key Laboratory of Surface Physics, Fudan University, Shanghai 200433, China*
[3]*Institut für Experimentelle und Angewandte Physik, Universität Regensburg, Regensburg 93040, Germany*
[4]*Beijing National Laboratory for Condensed Matter Physics, Institute of Physics, Chinese Academy of Sciences, Beijing 100190, China*
[5]*Key Laboratory for Magnetism and Magnetic Materials of Ministry of Education, School of Physical Science and Technology, Lanzhou University, Lanzhou 730000, China*
[6]*School of Information Science and Technology, Shanghai Technology University, Shanghai 201210, China*
[7]*Physik-Department, Technische Universität München, Garching 85748, Germany*

Magnetic skyrmions have significant potential for applications in storage and logic devices, but the ability to control skyrmion motion is key to their success. To realize controlled skyrmion motion, vertical spin current-driven methods employing, e.g., the spin Hall or inverse spin galvanic effect, are efficient; thus, magnetic heterostructures featuring large spin-orbit torques are appealing. In this paper, we report on the observation of room-temperature magnetic skyrmions in Pt/Co/W multilayers. The interfacial Dzyaloshinskii-Moriya interaction was estimated to be 0.19 ± 0.05 mJ/m^2 based on the asymmetric domain-wall motion occurring upon the application of in-plane magnetic fields. The evolution of the magnetic structures from labyrinth domains to skyrmions with diameters of around 145 nm under magnetic fields was observed by performing Lorentz transmission electron microscopy. The skyrmion nucleation fields could be tuned by varying the repetition number. Large spin Hall angle systems such as Pt/Co/W multilayers are appealing for achieving current-driven skyrmion motion in future racetrack and logic applications.

I. INTRODUCTION

Magnetic skyrmions are chiral spin textures, which are considered to be potential candidates for future ultra-low-power spintronics storage [1–9], benefitting from small particle size, topological protection, and low driving current density thresholds. To date, magnetic skyrmions have been observed in noncentrosymmetric bulk materials, ultrathin films in which the interface breaks the symmetry, and artificial structures [10–19]. Among them, systems with broken interfacial symmetry attract enormous attention, because the skyrmion phase can exist in these systems at room temperature and in regions with low magnetic fields. These systems have been intensively studied experimentally with the objective of realizing room-temperature skyrmions, current-driven skyrmion motion, and electrical detection of single skyrmions [16,17,20]. The obtained results are crucial for the development of functional skyrmion-based devices.

The realization of magnetic skyrmion devices strongly depends on the ability to create and move skyrmions with low power consumption. In a skyrmion track device [5,21], the energy cost of skyrmion motion is critical. Although various methods of achieving efficient skyrmion motion have been proposed theoretically, only spin-polarized current-driven motion has been realized. Current-induced skyrmion motion is described by spin transfer torque (STT), which includes current in-plane STT (CIP-STT) and spin Hall effect STT (SHE-STT) [22–24]. SHE-STT is more efficient than CIP-STT with the same current density [22,24]. The SHE converts the horizontal charge current into a vertical pure spin current in a heavy metal. From $\theta_{\mathrm{SH}} = |J_s|/|J_c|$ [25,26], where θ_{SH} is the spin Hall angle, J_c is the charge current density, and J_s is the spin current density, the conversion efficiency depends on the spin Hall angle of the heavy metal. Consequently, skyrmions that exist in large spin Hall angle materials are appealing for skyrmion-based device applications.

To date, magnetic skyrmions in systems with broken interfacial symmetry have been realized in Pt/Co/Ir [27,28], Pt/Co/Ta [29], Ta/CoFeB/TaOx [16], etc. A high skyrmion velocity of about 100 m/s upon the application of $\sim 5 \times 10^{11}$ A/cm^2 was achieved in Pt/CoFeB/MgO multilayers [29], while 50 and 30 m/s have been reported in Pt/Co/Ta and Pt/Co/Ir, respectively. The longitudinal skyrmion velocity can be written as $v_x = \frac{\delta}{1+\delta^2} \frac{F_{\mathrm{SHE}}}{G_z}$ [24,30], where δ is related to the dissipative tensor and Gilbert damping, G_z is the gyro vector, and $\boldsymbol{F}_{\mathrm{SHE}}$ is the force caused by SHE-STT. $\boldsymbol{F}_{\mathrm{SHE}}$ is expressed as $\pm \frac{\hbar}{2e} \pi j \theta_{\mathrm{SH}} b \boldsymbol{e}_z \times \boldsymbol{e}_p$ [24,30], where j is the current density, b is a skyrmion characteristic length [half its perimeter when the skyrmion radius is much

* Corresponding author: na.lei@buaa.edu.cn
† christian.back@ur.de
‡ weisheng.zhao@buaa.edu.cn

larger than the length scale of a domain-wall (DW) width], e_z is the vertical direction in the laboratory frame, and $e_p = n \times j$, with n being the outer normal to the SHE layer at the interface considered. Therefore, the longitudinal velocity is proportional to the spin Hall angle (θ_{SH}) and inversely proportional to the damping. The damping constant is much lower in CoFeB than in Co films, which presumably leads to the high skyrmion speed. For relatively the same damping constants in both Pt/Co systems, the large spin Hall angle in current-driven skyrmion motion plays an important role. To achieve more rapid skyrmion motion, such as for DWs, larger spin Hall angle systems are necessary. In this paper, we report on a candidate thin-film structure for magnetic skyrmions in Pt/Co/W multilayers. In this structure, W has a very large negative spin Hall angle ($\sim -0.33 \pm 0.06$) [31] and Pt has a positive spin Hall angle ($\sim +0.11 \pm 0.08$) [32], which is much larger than Pt/Co/Ta systems (the spin Hall angle of Ta is $\sim -0.12 \pm 0.04$) [33]. Note that the spin Hall angles of the heavy metals depend on their crystalline structure and film quality [34]; here the β phase W is controlled during deposition. Furthermore, Pt/Co/W systems show a great reduction of damping constant compared to Pt/Co/Ta [35]. As we will show, the skyrmion size is about 145 nm, which is smaller than that in a Pt/Co/Ta multilayer. Thus, a higher speed skyrmion motion can be expected in this system.

II. EXPERIMENTAL DETAILS

The samples were grown by magnetron sputtering at a base pressure greater than 3×10^{-8} Torr. The sample structure was (Si/SiO$_2$)/Ta (5 nm)/Pt (5 nm)/Co (1.8 nm)/W (1 nm)/Pt (1 nm). The growth conditions including pressure and deposition rate were well controlled to ensure the growth of the β phase W based on previous reports [36–38]. The hysteresis loops were measured by performing vibrating sample magnetometry with both in-plane and perpendicular magnetic fields, as shown in Fig. 1(a). To extract the effective anisotropy constant K_{eff}, initial magnetization loop measurements were performed along both field directions and are depicted in the inset. The saturation magnetization moment M_s and K_{eff} were determined to be 7.4×10^5 A/m and 0.13 MJ/m^3, respectively.

III. RESULTS AND DISCUSSION

The Dzyaloshinskii-Moriya interaction (DMI) in structures with interfacial asymmetry favors noncollinear spin arrangement. The corresponding Hamiltonian is [24,39]

$$\mathcal{H}_{DMI} = \boldsymbol{D}_{ij} \cdot (\boldsymbol{S}_i \times \boldsymbol{S}_j), \tag{1}$$

where $\boldsymbol{D}_{ij}$ is the DMI vector and $\boldsymbol{S}_i$ and $\boldsymbol{S}_j$ are two neighboring spins in magnetic materials. It has been reported that the DMI coefficients D_1 (for the W/Co interface) and D_2 (for the Pt/Co interface) are both positive, and that D_2 is larger than D_1 [24,40,41]. Therefore, in a trilayer structure, for example Pt/Co/W, the DMI will contain contributions from both the Pt/Co and Co/W interfaces, and the effective coefficient is expected to be positive but smaller than D_2. A schematic of the structure of Pt/Co/W is shown in Fig. 1(b). In this structure, qualitative and quantitative DMI evaluation was performed

through asymmetric DW motion with in-plane fields. Room-temperature Kerr microscopy with an in-plane electromagnet and a perpendicular Helmholtz coil was performed to study the DW motion. The magnets were well aligned to avoid any crosstalk.

To investigate the DW motion in the creep regime, we varied the perpendicular pulse fields to measure the DW velocity with a pulse width of 25 ms, and the results are shown in Fig. 1(c). The linear relation between the DW velocity in logarithmic scale and $H_z^{-1/4}$ is clearly observable. This finding is consistent with the well-known Arrhenius-type relation [42,43]

$$\nu(H_z) = \nu_0 \exp \left[-\kappa H_z^{-1/4} \right], \tag{2}$$

where ν_0 is a velocity prefactor and κ is a function related to the elastic, pinning potential, and thermal energies.

In the DW asymmetric motion experiment, the in-plane constant field and perpendicular pulse field were applied simultaneously to drive the DW motion. To extract the accurate DW speed, the duration time of the perpendicular pulse field was strictly controlled. We fixed the pulse width as 25 ms, and varied the number of the pulses to ensure that the fields applied in each pulse were the same. Additionally, the pulse profile was monitored and the rise time is about 0.37 ms, which is negligible compared to the pulse width of 25 ms [44]. The perpendicular field was kept as 125 Oe for both the nucleation domain and DW motion, which is in the creep regime of DW motion. The in-plane magnetic field was varied from +900 to −900 Oe. The differential Kerr images are shown in the insets in Fig. 1(d) with in-plane fields of −550, 0, and +600 Oe from left to right, respectively. In the inset images, the dark areas indicate the domain expansion under the perpendicular pulse fields together with in-plane bias field applied. The asymmetric motion of the left and right DWs with in-plane fields is evident, which indicates that DMI exists in the structure of Pt/Co/W. Note that the DW boundaries are not smooth, which is due to the magnetic irregularities for nucleation and/or DW pinning sites in thick film layers [45,46].

The DW velocities of the left and right sides were extracted and are plotted as functions of the in-plane field in Fig. 1(d). The data point is the average value of five repeating experiments to reduce the uncertainty from the irregular boundary of the magnetic domains, and the error bar shown in Fig. 1(d) is standard deviation. The minimum velocity for the left (right) direction appears at an in-plane bias field of 250 Oe (−250 Oe), which means that the DMI equivalent field H_{DMI} is around 250 Oe. The relation between H_{DMI} and D is [43]

$$H_{DMI} = \frac{D}{\mu_0 M_s \lambda}, \tag{3}$$

where D is the DMI coefficient and λ is the DW width. $\lambda = \sqrt{\frac{A}{K_{eff}}}$, where A is the exchange constant. Inserting $M_s = 7.4 \times 10^5$ A/m, $K_{eff} = 0.13$ MJ/m^3, and $A = 1.3 \times 10^{-11}$ J/m [47] into Eq. (3), the DMI constant in this Pt/Co/W trilayer was calculated. Theoretical fits were also conducted based on the DW velocity in the creep regime with DM interaction in the system for verification [48], and the DMI constant was estimated as 0.19 ± 0.05 mJ/m^2. This
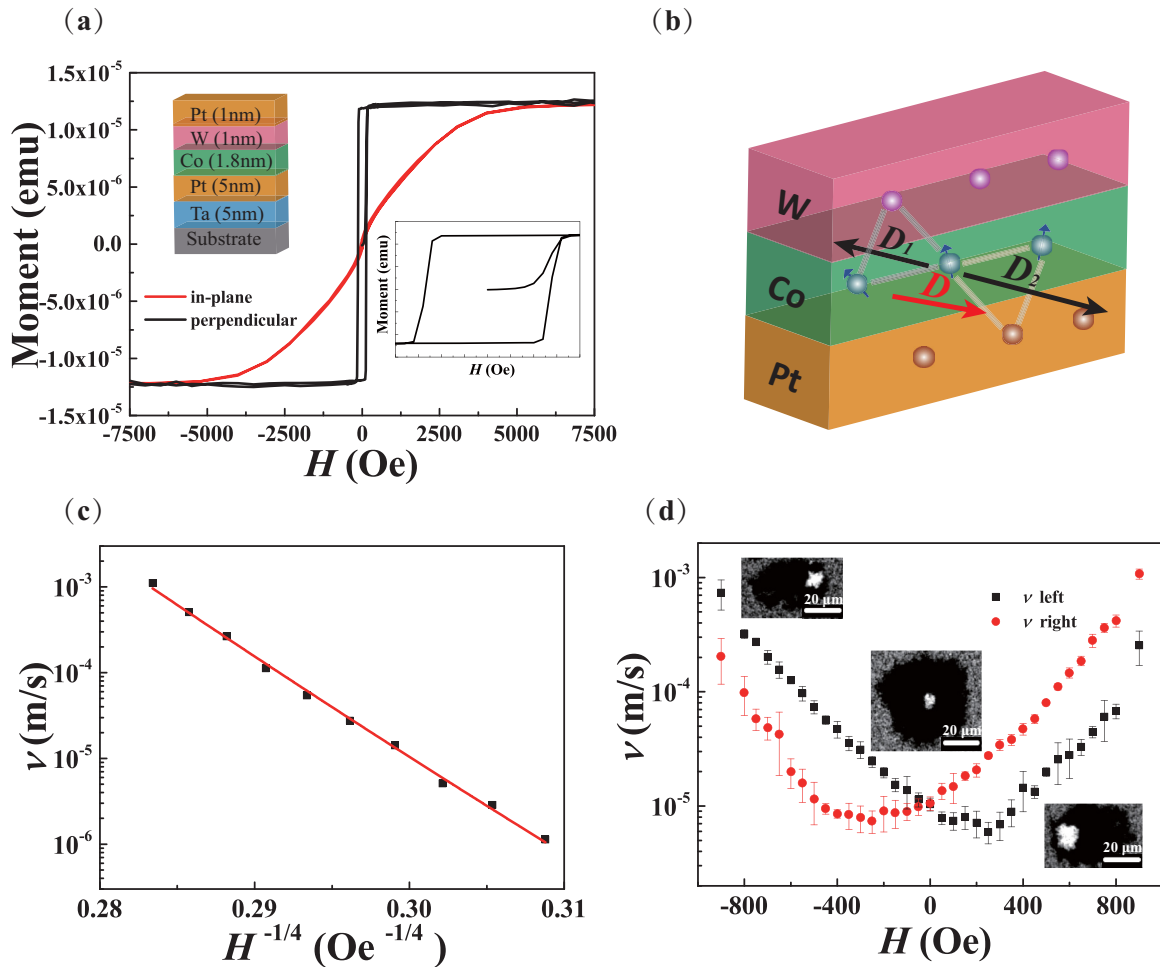
FIG. 1. (a) Sample structure and hysteresis loops along in-plane and perpendicular directions. (b) Schematic of the DMI in a Pt/Co/W film structure. (c) DW velocity in Pt/Co/W film as a function of the perpendicular magnetic field with zero in-plane field. (d) DW velocity along the in-plane direction as a function of the in-plane bias field, a pulsed perpendicular magnetic field with 125 Oe was induced simultaneously. Insets: Differential Kerr images of domains under perpendicular pulse fields together with in-plane bias fields. In-plane fields and perpendicular pulse field durations are −550 Oe, 0.275 s; 0 Oe, 2.2 s; and +600 Oe, 0.25 s (left to right).

value is relatively small, presumably due to the relatively thick Co layer (1.8 nm) [17,43,49].

To realize skyrmions in Pt/Co/W systems, the trilayer structure was repeated to increase the contribution of the demagnetizing field. Figure 2(a) shows the perpendicular hysteresis loop of a five-period $[Pt/Co/W]_5$ multilayer measured by polar magneto-optical Kerr effect (MOKE). Increasing the number of Pt/Co/W periods reduced the effective perpendicular magnetic anisotropy due to the competition between the perpendicular anisotropy and the increasing superimposed interfacial roughness. Simultaneously, the dipolar energy was enhanced. Consequently, the perpendicular magnetic hysteresis loops clearly exhibit sheared shapes, as is typical for a perpendicularly magnetized system that decays into labyrinth domains [11,29]. Similar loop changes have also been observed as a result of domain propagation in multiperiod Co/Pt structures [50]. Domain nucleation and reversal with increasing number of periods, resulting in the transformation of nucleation and saturation fields, have been identified in hysteresis loops [50,51]. If the structures also have proper DMI, which introduces chirality into the DWs,

magnetic skyrmions can be expected to appear when the labyrinth domain shrinks into small bubbles.

To observe the skyrmion phase in Pt/Co/W multilayers, Lorentz transmission electron microscopy (LTEM) was performed on layers grown on a 20-nm-thick SiN_x membrane substrate. The experiment was conducted at room temperature with a 20° tilt of the sample normal with respect to the beam axis and the externally applied magnetic field. The images in Figs. 2(b)–2(e) show the magnetic contrast images obtained with different external fields and each spans a field of view of $\sim 4 \times 4 \, \mu m^2$. The magnetic structure in the multilayer is determined by the competition among the energy terms, including the exchange interaction, magnetic anisotropy, DM interaction, and dipole-dipole energies. The increased dipole-dipole interactions in the repeated Pt/Co/W trilayers tend to feature a labyrinth domain in weak magnetic fields. Due to the Zeeman interaction, an increase in the magnetic field favors stripe domains with parallel magnetization, which consequently start to expand [10,50]. The unfavored antiparallel domains shrink and are pinched off, leaving behind isolated stripes. When the endings of such a stripe approach each
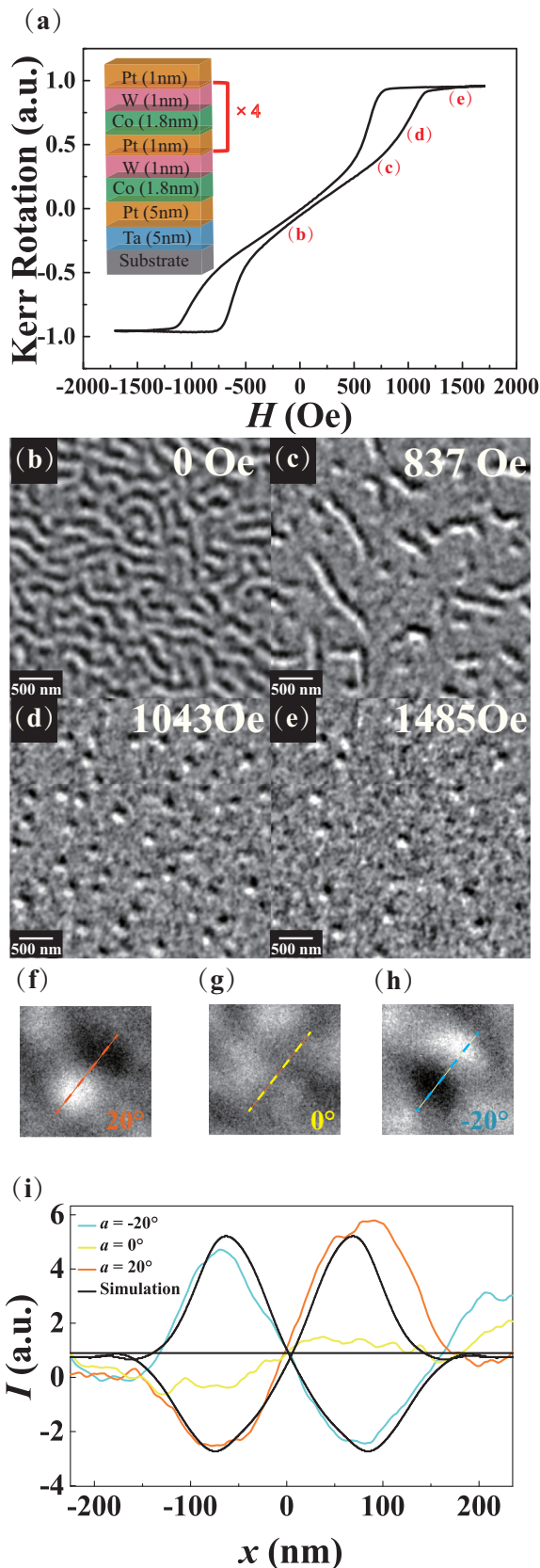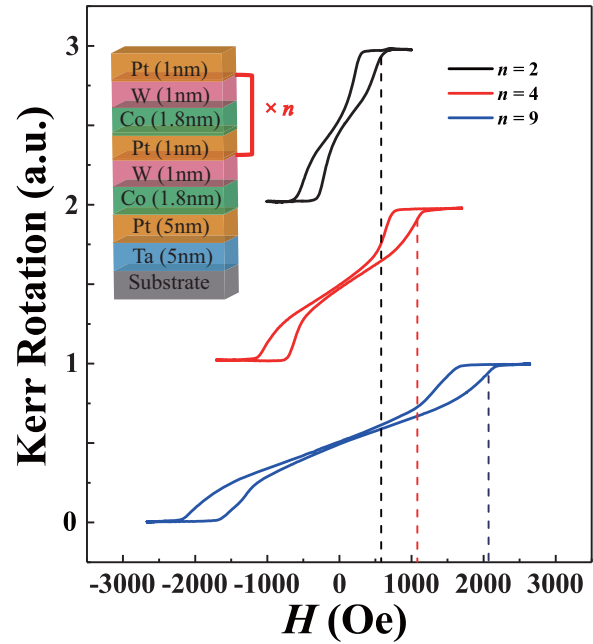
FIG. 3. Normalized polar hysteresis loops of multiperiod Pt/Co/W measured by MOKE. The loops are shifted vertically for clarity. The dashed lines indicate the threshold magnetic fields of the magnetic skyrmions.

other, the topological energy barrier stabilizes a skyrmion. A mixture of skyrmions and stripes can be seen in Fig. 2(c). When another increase in the magnetic field overcomes any pinning potential of the remaining stripes, the evolution to the skyrmion phase is completed. Finally, the skyrmion density slowly decreases upon further field increase since the uniform domain is preferred above the saturation field, as shown in Figs. 2(d) and 2(e).

The origin of the antisymmetric exchange interaction allows for different kinds of DM interactions that can lead to skyrmions with Bloch and Néel configurations or even antiskyrmions [24,27,28,52]. The interfacial DMI usually entails Néel-type configurations. To confirm the existence of Néel-type skyrmions in the Pt/Co/W multilayers, the sample was tilted to ±20° with respect to the electron beam, as shown in Figs. 2(f) and 2(h). The image obtained with normal electron-beam incidence is presented in Fig. 2(g) for the same skyrmion. Obviously, the skyrmion exhibits a dark to bright contrast profile along the tilting direction that is mirrored when the tilt has the opposite sign. Without tilting, practically no magnetic contrast can be seen. The respective line profiles are plotted in Fig. 2(i) and clearly show the contrast reversal.

To estimate the skyrmion size, LTEM contrast simulations were conducted [53–55]. For these simulations, the spin structure of a Néel skyrmion with a diameter of 145 nm was generated. The simulations were performed with an experimental defocus of 2.95 mm, a magnetization of 1.4×10^6 A/m, and the various tilt angles. Considering the crystalline

FIG. 2. (a) Sample structure and polar hysteresis loop measured by MOKE for a sample with five periods of Pt/Co/W. (b–e) LTEM images of the five-period Pt/Co/W sample for different applied magnetic field strengths, as indicated in the top right of each image. (f–h) LTEM images of magnetic skyrmions with tilting angles of (f) +20°, (g) 0°, and (h) −20°. (i) Line profiles extracted from the LTEM images in (f–h).

background, the resulting line profiles match the experimental data sufficiently well, as can be seen in Fig. 2(i).

In the Pt/Co/W multilayer films, the increasing dipole-dipole interaction upon repetition of the trilayer structure induces a labyrinth domain structure in the ground state. The additional Zeeman energy from the applied field breaks up the labyrinth domain to form skyrmions and finally a uniform domain structure. The applied field required to reach the skyrmion state is strongly related to the dipole energy, which can be tuned by adjusting the number of repetitions n of the trilayer structure. We varied n from 2 to 9, and the corresponding hysteresis loops measured using the polar MOKE are shown in Fig. 3. All three loops exhibit typical sheared shapes, while the saturation field increases with increasing number of repetitions, as indicated by the vertical dashed lines. The field at which the skyrmion phase appears also changes dramatically; there is a decrease of around 75% between those of the samples with ten and three periods. This has been confirmed by magnetic force microscopy measurements with varying the magnetic fields [56]. Thus, this technique is an effective alternative method for realizing magnetic skyrmions in the ground state.

IV. CONCLUSION

In summary, Pt/Co/W multilayers were experimentally explored and proposed as a skyrmionic material candidate in this paper. The perpendicular magnetic anisotropy of the Pt/Co/W multilayers was effectively tuned by varying the number of repetitions, providing an alternative method of controlling

the field to produce skyrmions. In the Pt/Co/W multilayers, the existence of magnetic skyrmions was indicated by the magnetic hysteresis loops and further confirmed by the LTEM observations. By comparing the asymmetry of the DW velocity along/opposite to the in-plane bias magnetic field, the DMI in Pt/Co/W was quantitatively analyzed by conducting both experiments and calculations. In addition, the existence of a Néel-type spin texture was ensured by performing LTEM observations while tilting the sample in opposite directions. As Pt/Co/W multilayers have larger spin-orbit torque from both the Pt/Co and Co/W interfaces, highly efficient current-induced skyrmion motion can be expected in our structures, which may offer a means of manipulating skyrmions. By utilizing both the perpendicular magnetic anisotropy and interfacial DMI in the Pt/Co/W structure, we expect efficient driving and manipulation of magnetic skyrmions to be possible, which may lead to ultra-low-power applications in future skyrmion-based memory and logic spintronics devices.

[1] T. H. R. Skyrme, Nucl. Phys. **31**, 556 (1962).

[2] U. K. Rößler, A. N. Bogdanov, and C. Pfleiderer, Nature (London) **442**, 797 (2006).

[3] X. Z. Yu, Y. Onose, N. Kanazawa, J. H. Park, J. H. Han, Y. Matsui, N. Nagaosa, and Y. Tokura, Nature (London) **465**, 901 (2010).

[4] Y. Nakatani, M. Hayashi, S. Kanai, S. Fukami, and H. Ohno, Appl. Phys. Lett. **108**, 152403 (2016).

[5] A. Fert, V. Cros, and J. Sampaio, Nat. Nanotech. **8**, 152 (2013).

[6] W. Kang, C. Zheng, Y. Huang, X. Zhang, Y. Zhou, W. Lv, and W. Zhao, IEEE Electron Device Lett. **37**, 924 (2016).

[7] Y. Huang, W. Kang, X. Zhang, Y. Zhou, and W. Zhao, Nanotechnology **28**, 08LT02 (2017).

[8] Z. Li, Y. Zhang, Y. Huang, C. Wang, X. Zhang, Y. Liu, Y. Zhou, W. Kang, S. Chandrashekhar Koli, and N. Lei, J. Magn. Magn. Mater. **455**, 19 (2018).

[9] M. Vousden, M. Albert, M. Beg, M.-A. Bisotti, R. Carey, D. Chernyshenko, D. Cortés-Ortuño, W. Wang, O. Hovorka, C. H. Marrows, and H. Fangohr, Appl. Phys. Lett. **108**, 132406 (2016).

[10] G. Yu, P. Upadhyaya, X. Li, W. Li, S. K. Kim, Y. Fan, K. L. Wong, Y. Tserkovnyak, P. K. Amiri, and K. L. Wang, Nano Lett. **16**, 1981 (2016).

[11] A. Soumyanarayanan, M. Raju, A. L. Gonzalez Oyarce, A. K. C. Tan, M.-Y. Im, A. P. Petrović, P. Ho, K. H. Khoo, M. Tran, C. K. Gan, F. Ernult, and C. Panagopoulos, Nat. Mater. **16**, 898 (2017).

[12] S. D. Pollard, J. A. Garlow, J. Yu, Z. Wang, Y. Zhu, and H. Yang, Nat. Commun. **8**, 14761 (2017).

[13] N. Romming, A. Kubetzka, C. Hanneken, K. von Bergmann, and R. Wiesendanger, Phys. Rev. Lett. **114**, 177203 (2015).

[14] T. Adams, S. Mühlbauer, C. Pfleiderer, F. Jonietz, A. Bauer, A. Neubauer, R. Georgii, P. Böni, U. Keiderling, K. Everschor, M. Garst, and A. Rosch, Phys. Rev. Lett. **107**, 217206 (2011).

[15] A. Tonomura, X. Yu, K. Yanagisawa, T. Matsuda, Y. Onose, N. Kanazawa, H. S. Park, and Y. Tokura, Nano Lett. **12**, 1673 (2012).

[16] W. Jiang, P. Upadhyaya, W. Zhang, G. Yu, M. B. Jungfleisch, F. Y. Fradin, J. E. Pearson, Y. Tserkovnyak, K. L. Wang, O. Heinonen, S. G. E. te Velthuis, and A. Hoffmann, Science **349**, 283 (2015).

[17] S. Jaiswal, K. Litzius, I. Lemesh, F. Büttner, S. Finizio, J. Raabe, M. Weigand, K. Lee, J. Langer, B. Ocker, G. Jakob, G. S. D. Beach, and M. Kläui, Appl. Phys. Lett. **111**, 022409 (2017).

[18] D. A. Gilbert, B. B. Maranville, A. L. Balk, B. J. Kirby, P. Fischer, D. T. Pierce, J. Unguris, J. A. Borchers, and K. Liu, Nat. Commun. **6**, 8462 (2015).

[19] B. F. Miao, L. Sun, Y. W. Wu, X. D. Tao, X. Xiong, Y. Wen, R. X. Cao, P. Wang, D. Wu, Q. F. Zhan, B. You, J. Du, R. W. Li, and H. F. Ding, Phys. Rev. B **90**, 174411 (2014).

[20] D. Maccariello, W. Legrand, N. Reyren, K. Garcia, K. Bouzehouane, S. Collin, V. Cros, and A. Fert, Nat. Nanotech. **13**, 233 (2018).

[21] W. Kang, Y. Huang, C. Zheng, W. Lv, N. Lei, Y. Zhang, X. Zhang, Y. Zhou, and W. Zhao, Sci. Rep. **6**, 23164 (2016).

[22] J. Sampaio, V. Cros, S. Rohart, A. Thiaville, and A. Fert, Nat. Nanotech. **8**, 839 (2013).

[23] J. Iwasaki, M. Mochizuki, and N. Nagaosa, Nat. Nanotech. **8**, 742 (2013).

[24] A. Fert, N. Reyren, and V. Cros, Nat. Rev. Mater. **2**, 17031 (2017).

[25] Y. Wang, P. Deorani, X. Qiu, J. H. Kwon, and H. Yang, Appl. Phys. Lett. **105**, 152412 (2014).

[26] K. Kouta, S. Hiroaki, M. Seiji, T. Kazuhito, and K. Shinya, Appl. Phys. Expr. **5**, 073002 (2012).

[27] C. Moreau-Luchaire, C. Moutafis, N. Reyren, J. Sampaio, C. A. F. Vaz, N. Van Horne, K. Bouzehouane, K. Garcia, C. Deranlot, P. Warnicke, P. Wohlhüter, J. M. George, M. Weigand, J. Raabe, V. Cros, and A. Fert, Nat. Nanotech. **11**, 444 (2016).

[28] K. Zeissler, M. Mruczkiewicz, S. Finizio, J. Raabe, P. M. Shepley, A. V. Sadovnikov, S. A. Nikitov, K. Fallon, S. Mc-Fadzean, S. McVitie, T. A. Moore, G. Burnell, and C. H. Marrows, Sci. Rep. **7**, 15125 (2017).

[29] S. Woo, K. Litzius, B. Krüger, M.-Y. Im, L. Caretta, K. Richter, M. Mann, A. Krone, R. M. Reeve, M. Weigand, P. Agrawal, I. Lemesh, M.-A. Mawass, P. Fischer, M. Kläui, and G. S. D. Beach, Nat. Mater. **15**, 501 (2016).

[30] A. Hrabec, J. Sampaio, M. Belmeguenai, I. Gross, R. Weil, S. M. Chérif, A. Stashkevich, V. Jacques, A. Thiaville, and S. Rohart, Nat. Commun. **8**, 15765 (2017).

[31] C.-F. Pai, L. Liu, Y. Li, H. W. Tseng, D. C. Ralph, and R. A. Buhrman, Appl. Phys. Lett. **101**, 122404 (2012).

[32] M. Althammer, S. Meyer, H. Nakayama, M. Schreier, S. Altmannshofer, M. Weiler, H. Huebl, S. Geprägs, M. Opel, R. Gross, D. Meier, C. Klewe, T. Kuschel, J.-M. Schmalhorst, G. Reiss, L. Shen, A. Gupta, Y.-T. Chen, G. E. W. Bauer, E. Saitoh, and S. T. B. Goennenwein, Phys. Rev. B **87**, 224401 (2013).

[33] L. Liu, C. F. Pai, Y. Li, H. W. Tseng, D. C. Ralph, and R. A. Buhrman, Science **336**, 555 (2012).

[34] X. Tao, Q. Liu, B. Miao, R. Yu, Z. Feng, L. Sun, B. You, J. Du, K. Chen, S. Zhang, L. Zhang, Z. Yuan, D. Wu, and H. Ding, Sci. Adv. **4**, eaat1670 (2018).

[35] B. Zhang, A. Cao, J. Qiao, M. Tang, K. Cao, X. Zhao, S. Eimer, Z. Si, N. Lei, Z. Wang, X. Lin, Z. Zhang, M. Wu, and W. Zhao, Appl. Phys. Lett. **110**, 012405 (2017).

[36] I. A. Weerasekera, S. I. Shah, D. V. Baxter, and K. M. Unruh, Appl. Phys. Lett. **64**, 3231 (1994).

[37] Q. Hao, W. Chen, and G. Xiao, Appl. Phys. Lett. **106**, 182403 (2015).

[38] Q. Hao and G. Xiao, Phys. Rev. Appl. **3**, 034009 (2015).

[39] S. Tacchi, R. E Troncoso, M. Ahlberg, G. Gubbiotti, M. Madami, J. Åkerman, and P. Landeros, Phys. Rev. Lett. **118**, 147201 (2017).

[40] A. Belabbes, G. Bihlmayer, F. Bechstedt, S. Blügel, and A. Manchon, Phys. Rev. Lett. **117**, 247202 (2016).

[41] J. P. Tetienne, T. Hingant, L. J. Martínez, S. Rohart, A. Thiaville, L. Herrera Diez, K. Garcia, J. P. Adam, J. V. Kim, J. F. Roch, I. M. Miron, G. Gaudin, L. Vila, B. Ocker, D. Ravelosona, and V. Jacques, Nat. Commun. **6**, 6733 (2015).

[42] S. Lemerle, J. Ferré, C. Chappert, V. Mathet, T. Giamarchi, and P. Le Doussal, Phys. Rev. Lett. **80**, 849 (1998).

[43] R. Soucaille, M. Belmeguenai, J. Torrejon, J. V. Kim, T. Devolder, Y. Roussigné, S. M. Chérif, A. A. Stashkevich, M. Hayashi, and J. P. Adam, Phys. Rev. B **94**, 104431 (2016).

[44] See Supplemental Material at http://link.aps.org/supplemental/10.1103/PhysRevB.98.174425 for the pulse profile of the Helmholtz coil.

[45] S.-B. Choe and S.-C. Shin, Appl. Phys. Lett. **80**, 1791 (2002).

[46] K. S. Lee, C. W. Lee, Y. J. Cho, S. Seo, D. H. Kim, and S. B. Choe, IEEE Trans. Magn. **45**, 2548 (2009).

[47] P. E. Tannenwald and R. Weber, Phys. Rev. **121**, 715 (1961).

[48] See Supplemental Material at http://link.aps.org/supplemental/10.1103/PhysRevB.98.174425 for theoretical fittings for DW velocity under in-plane magnetic fields, which include Refs. [43,57–61].

[49] I. Gross, L. J. Martínez, J. P. Tetienne, T. Hingant, J. F. Roch, K. Garcia, R. Soucaille, J. P. Adam, J. V. Kim, S. Rohart, A. Thiaville, J. Torrejon, M. Hayashi, and V. Jacques, Phys. Rev. B **94**, 064413 (2016).

[50] O. Hellwig, A. Berger, J. B. Kortright, and E. E. Fullerton, J. Magn. Magn. Mater. **319**, 13 (2007).

[51] C. Kooy and U. Enz, Philips Res. Rep. **15**, 7 (1960).

[52] A. K. Nayak, V. Kumar, T. Ma, P. Werner, E. Pippel, R. Sahoo, F. Damay, U. K. Rößler, C. Felser, and S. S. P. Parkin, Nature (London) **548**, 561 (2017).

[53] M. Beleggia, M. A. Schofield, Y. Zhu, M. Malac, Z. Liu, and M. Freeman, Appl. Phys. Lett. **83**, 1435 (2003).

[54] M. Mansuripur, J. Appl. Phys. **69**, 2455 (1991).

[55] T. Haug, S. Otto, M. Schneider, and J. Zweck, Ultramicroscopy **96**, 201 (2003).

[56] See Supplemental Material at http://link.aps.org/supplemental/10.1103/PhysRevB.98.174425 for magnetic force microscopy results with varying magnetic fields for different period skyrmion samples.

[57] S.-G. Je, D.-H. Kim, S.-C. Yoo, B.-C. Min, K.-J. Lee, and S.-B. Choe, Phys. Rev. B **88**, 214401 (2013).

[58] J. H. Franken, M. Herps, H. J. M. Swagten, and B. Koopmans, Sci. Rep. **4**, 5248 (2014).

[59] E. Jué, C. K. Safeer, M. Drouard, A. Lopez, P. Balint, L. Buda-Prejbeanu, O. Boulle, S. Auffret, A. Schuhl, A. Manchon, I. M. Miron, and G. Gaudin, Nat. Mater. **15**, 272 (2016).

[60] C. A. Akosa, I. M. Miron, G. Gaudin, and A. Manchon, Phys. Rev. B **93**, 214429 (2016).

[61] D.-Y. Kim, D.-H. Kim, and S.-B. Choe, Appl. Phys. Express **9**, 053001 (2016).